Development of Pathological Super-resolution Images using Artificial Intelligence based on Whole Slide Image

Yang Deng
Sichuan University West China Hospital
Min Feng
Sichuan University West China Hospital
Yong Jiang
Sichuan University West China Hospital
Yanyan Zhou
Sichuan University West China Hospital
Hangyu Qing
Sichuan University West China Hospital
Fei Xiang
Chengdu Knowledge Vision Science and Technology Co. Ltd.
Yizhe Wang
Chengdu Knowledge Vision Science and Technology Co. Ltd
Ji Bao (baoji@scu.edu.cn)
Sichuan University West China Hospital
Hong Bu
Sichuan University West China Hospital

Research

Keywords: Super-resolution, Whole Slide Image, Artificial Intelligence, Adult Granulosa Cell Tumor, Uterine Leiomyosarcoma

Posted Date: February 20th, 2020

DOI: https://doi.org/10.21203/rs.2.24125/v1

Abstract

Background: Pathology plays a very important role in the cancer diagnosis, as the gold standard for the identification of tumors. The rapid development of digital pathology (DP) which based on Whole Slide Image (WSI) has led to many improvements in telepathological consultation, digital management, and computer-assisted diagnosis by artificial intelligence (AI). In DP, the common digitization strategy is to scan the pathology slice with X20 or X40 objective. Usually, the X40's WSI is 4 times bigger than the X20's, and obviously, the storage space and transmission time of the data should be 4 times. These increased costs will be great negative factor in the popularization of DP. But at the same time, some cases have to use the high magnification WSI for reliable diagnosis.

Methods: In this article, we present a novel super-resolution process which could be used for WSI through Deep Learning. This process powered by AI, have the ability to switch X20 WSI to X40 without loss of whole and locally features. Furthermore, we collect the examples of WSI data of patients with 100 uterine leiomyosarcoma and adult granulosa cell tumor (AGCT) of ovary respectively, which are used to test our super-resolution process.

Results: We used the peak signal-to-noise ratio (PSNR), the structural similarity (SSIM), and the Blind/Referenceless Image Spatial QUality Evaluator (BRISQUE) to test the resulting X40 WSI synthesized by the super-resolution (SR), which were 42.03, 0.99 and 49.22 . Then, we tested our SR images from subjective evaluation of the pathologist's perspective, and tested that if the pathologists could objectively distinguish the images between SR and high-resolution (HR), to further confirm the consistency between our SR images and the real HR images.

Conclusions: The testing results indicate that the X40 WSI synthesized by the super-resolution matches the performance of the one generated from the X40 objective in diagnosis of both tumors. We believe that this is a reliable method can be used in a variety of tumors' digital slides, and will be available for a large scale in clinical pathology as an innovative technique.

Introduction

Pathology is an important way to diagnosis of diseases, in particular in malignant tumours, the whole slide image, which meet the characteristics of high definition, high speed, and high throughput screening, provides the possibility for digitization of traditional pathology slice, which lays a good foundation for the development and application of digital pathology (DP) [1–2]. With the development of DP, the storage and transmission of the pathological image gets easier, which has led to many improvements in telepathological consultation, digital management, and computer-assisted diagnosis by artificial intelligence (AI). There have been reportedly more than 1,000,000 cases of telepathological consultation in China of the last 10 years. [3]

In digital pathology, the common digitization strategy is to scan the pathology slice with X20 or X40 objective, the data generated by scan is called WSI (or digital slide). Usually, X40's WSI is 4 times bigger

than the X20's which from the same slice, and obviously, the storage space and transmission time of the data should be 4 times. These increased costs will be great negative factor in the popularization of DP. Although many lesions can be diagnosed at low or medium magnification, in some cases, even experienced pathologists need to observe cells and cell nuclear morphology at high magnification to further confirm the diagnosis. For example, the dusty cytoplasm is often characterized by small cell neuroendocrine carcinoma, the longitudinal nucleus has a great role in the diagnosis of Langerhans histiocytosis and ovarian granulosa cell tumor, the obvious mitotic has a good predictive effect on the diagnosis and differential diagnosis of uterine leiomyosarcoma. In order to provide more clear and identifiable evidence for the diagnosis of tumors, whether it is an optical image or a digital image at a high magnification (x40), it is necessary to meet the high requirements of the pathologist to see the details in the nucleus. In this article, we present a novel super-resolution(SR) process which could be used for WSI through Deep Learning.

For super-resolution imaging, deep learning techniques were recently developed for CT and MRI with a great success [4], there were some early attempts with a 3D convolutional neural network, generative adversarial network (GAN), and densely connected network [5–7]. Thus, the super-resolution techniques have been used and shown super values in imaging[8], and we expect the same in digital pathology.

Materials And Methods

In the present study, we use adult granulosa cell tumor (AGCT) of ovary and uterine leiomyosarcoma as two application scenarios to test our resolution process. AGCT is a low-grade malignant neoplasm with a significant propensity for late recurrence and metastasis[9]. Histologically, granulosa cell tumors (GCTs) divided into adult and juvenile, the former accounted for 95% of all GCTs [9–10]. Although some clinical manifestations such as estrogen stimulation and related hormone levels have an auxiliary role in the diagnosis of this tumor, the final diagnosis still depends on the traditional histopathological examination under light microscopy. Microscopically, tumor cells are arranged in trabecular, island-like, pseudo-adenoid, vesicular or solid lamellae. Due to its variable histological features and various forms often mixed in the same tumor, this undoubtedly caused some difficulties in diagnosis of AGCT. A large number of studies have shown that the Call-Exnar body and coffee bean-like nucleus or longitudinal nucleus are the characteristic changes in typical AGCT, which is an important suggestion for the diagnosis of ovarian adult granulosa cells [10]. Thus, to make the diagnosis more accurate, it is necessary for pathologists to see the details or features of nucleus under x40 magnification images.

Uterine leiomyosarcoma is the most common uterine sarcoma with high malignancy and poor prognosis. According to the diagnostic criteria for histopathology developed by Bell et al [11]: (1) oderate – diffuses atypia of tumor cells with obvious necrosis; (2) oderate – diffuses atypia of tumor cells without obvious necrosis, mitotic figures ≥ 10 / 10 HPF; (3) mildly atypia of tumor cells with obvious necrosis, mitotic figures are ≥ 10/10 HPF. The diagnosis of uterine leiomyosarcoma from histological perspective requires careful determination of three factors: coagulative necrosis, cell atypia, and mitotic index. The mitotic

index requires the pathologist to count at least 4 groups of 10 high power fields in areas where mitotic activity is active. Therefore, clear and high-resolution x40 magnification images are a basic prerequisite for pathologists to distinguish mitotic figures from apoptotic cells, denatured cell nuclei and nuclear debris.

We selected 45 cases of ovarian adult granulosa cell tumor and 32 cases of uterine leiomyosarcoma diagnosed from department of pathology, West China Second University Hospital, Sichuan University. All cases with no history of cancer and did not receive radiotherapy before surgery. Specimens were fixed with 4% neutral formaldehyde, conventional paraffin-embedded, 4 μm thick sections, HE staining, and light microscopy examination. All the HE slides were reviewed by 2 senior pathologists. At last, a total of 100 HE slides from 45 cases of ovarian AGCT and 100 HE slides from 32 cases of uterine leiomyosarcoma were included. All the 200 HE slides were made into full digital scanning section WSI by Hamamatsu Optics' NanoZoomer 2.0HT digital section scanner, the scanning magnification was 20 times objective and 40 times objective.

With the development of AI, deep learning with deep convolutional neural networks (CNNs)[12] has been shown to be a powerful algorithm for advancing biomedical image analysis[13 – 14]. By studying the development and progress in the field of Single Image Super-Resolution(SISR), we find that in these two years deep learning methods are obviously superior to the traditional ones in terms of peak signal-to-noise ratio (PSNR) and structural similarity (SSIM). Our goal is to zoom in 40 × from 20×, so we can adopt a single-scale model. For further considering the effect and computation comprehensively, we finally adopt the champion scheme named Enhanced Deep Super-Resolution network (EDSR) on New Trends in Image Restoration and Enhancement (NTIRE) 2017 Challenge on Single-Image-Super-Resolution (SISR).

EDSR is a kind of generative network based on sample learning. The general process is that firstly to get the low-resolution(LR) image down-sampled by interpolation from high-resolution (HR) image, as the LR input of a convolutional neural network(CNN), and the original image will be as the HR input of a CNN; then a large number of such paired samples are used to train the network so as to establish the end-to-end mapping relationship between the LR image and its corresponding HR image; and finally the mapping relationship is used to create a super-resolution(SR) image from LR image.

The author of EDSR constructs the model baseline with residual blocks, whose structure is similar to that of SRResNet[15]. However, the EDSR does not have the Rectified Linear Unit (ReLU) activation layers outside the residual blocks[20]. Moreover, the baseline model does not have residual scaling layers and includes only 64 feature maps for each convolution layer.

Super-resolution involves up-sampling operation of image resolution. The Super-Resolution Convolutional Neural Network (SRCNN) [16] applied convolution layers on the pre-upscaled LR image. It is inefficient because all convolutional layers have to compute on high-resolution feature space, yielding much more computation than on low-resolution space. To accelerate processing speed without loss of accuracy, Fast Super-Resolution Convolutional Neural Network (FSRCNN) [17] utilized parametric deconvolution layer at

the end of SR network, making all convolution layers compute on LR feature space. Another non-parametric efficient alternative is pixel shuffling [18] (a.k.a., sub-pixel convolution). Pixel shuffling is also believed to introduce less checkerboard artifacts than the deconvolutional layer. We also used the pixel shuffling as the up-sampling operation.

We used the adult granulosa cell tumor images and the leiomyosarcoma images as our datasets (Fig. 1a-b). We get a large of training patches with size of 512 × 512 as the HR images randomly spliting from each training Whole-Slide Imaging(WSI) and validating patches are from each validating WSI and testing patches are from each testing WSI.

Due to computational resources, we just use the baseline model of EDSR, and the specific parameters in training are listed in Table 1. When training, we use the RGB input patches of size 256 × 256 from LR image with the corresponding HR patches. The 512 × 512 RGB input patches from HR image and its bilinear down-sampled image will be as the training output-input pairs. We pre-process all the images by subtracting the mean RGB value based on the default settings. We also train our networks using L1 loss instead of L2, because L1 loss can provides better convergence than L2 as far as we know. We used both the granulosa cell tumor and the leiomyosarcoma output-input pairs. After a few training sessions, the final training loss curve is shown in Fig. 1c and the PSNR curve in validating dataset is shown in Fig. 1d. The last training used the best model before as the pre-trained model.

Results

We applied our trained model to the testing dataset including 2000 images with benchmark. We test two kinds of LR input with size of 256 × 256, one is bilinear down-sampled images from 40 × HR images (named sr_bilinear_as_lr_input), and another is directly from the 20 × images in WSI (named sr_self_as_lr_input). The mean PSNR and SSIM values between the SR images and HR images from testing dataset are listed in tabel 2. In general, the larger the PSNR or SSIM value is, the better quality the image has. PSNR value takes the infinite and SSIM value tasks 1.0 when two compared images are just the same. Some images results are shown in Fig. 2. We can conclude that our SR results are extremely similar to the HR images. To a large extent, we have achieved super-resolution reconstruction of the images.

We also applied our model to another dataset including 1000 images with approximate benchmark in which LR images with size of 256 × 256 are from the true 20 × WSI and HR images with size of 512 × 512 are from other true 40 × WSI. Some images results are shown in Fig. 3. The LR images are not down-sampled from HR images and they come from different WSI. Although we get the similar-pair images based on manual registration method as possible as we can, they do not have one-to-one correspondence in pixel spatial position. We couldn't use the PSNR or SSIM metrics to evaluate the results. We used another evaluation method named Blind/Referenceless Image Spatial QUality Evaluator (BRISQUE)[22], which is a kind of no-reference image quality assessment. That is to say, it just needs one image as input and the image quality score as the output. In general, the score is between 0 and 100, and the smaller the

score is, the better quality the image has. The mean BRISQUE scores of the HR images and the SR images related to Bicubic and ours on this testing dataset are listed in tabel 3. The average calculation time of our model for each image is about 2.5 milliseconds on GPU. From the results, we can see that the quality of our results are better than the SR images up-sampled by Bicubic, even better than the HR images. To a large extent, we have achieved super-resolution reconstruction of the images and our model can be applied to the true 20 × WSI to reconstructing 40 × WSI.

In order to further observe the texture details of SR images, we create two new test datasets, including 192 nuclear division images and 546 nuclear groove images with size of 32 × 32, which are annotated by doctors. Some images results are shown in Fig. 4 and the mean BRISQUE scores of the HR images and the SR images with Bicubic and ours are listed in tabel 4. From the results, we can also see that the quality of our results are better than the SR images up-sampled by Bicubic, even better than the HR images. To a large extent, our results can be used directly for subsequent tasks in these datasets.

Then, we tested the subjective evaluation of our SR images from the pathologist's perspective. We selected 1000 images from each of uterine leiomyosarcoma and adult granulosa cell tumor of ovary, and provided HR images and our SR images respectively. Two pathologists (intermediate titles) evaluated the SR images' authenticity subjectively, and considered whether the quality of the SR images are adequate for routine usage (diagnostic confidence), the results are shown in Table 5. In addition, we extracted 200 images from each of the two tumors, provided HR images and our SR images respectively but without any tags or comments, and let the pathologist to determine which are the true images (HR images). The test results showed that the probability of the two pathologists could accurately select the real images was 51.75% and 54.25% respectively (Table 6), which objectively proved that the pathologists could hardly distinguish the difference between these two kinds of images, and further confirmed the consistency between our SR images and the real HR images.

Discussion

The testing results indicate that the quality of our SR images reconstructed from true LR images are better than the SR images up-sampled by Bicubic, even better than the HR images whether from the perspective of vision or evaluation values, and the X40 WSI synthesized by the super-resolution matches the performance of the one generated from the X40 objective in diagnosis of both tumors. Based on this, we believe that the super-resolution technology is a reliable method in telepathological consultation, to improve diagnostic accuracy, reducing time and storage cost, and play an irreplaceable role in diseases which must be diagnosed at high magnification.

However, in this article, the super-resolution technology still has some problems and limitations. First, all we did is double zoom, if the magnification factor is larger such as × 4 or × 8, the restoration of details is not so good. Second, we just applied the baseline model to our task due to limited computing resources. The last, the model we have trained only applies to uterine leiomyosarcoma and adult granulosa cell

tumor (AGCT) of ovary, and we need more data for transfer learning if we want to apply this model to other diseases.

Inspiringly, the super-resolution algorithms are also improving, the authors[15] of the EDSR proved experimentally that the processing effect can be improved if the network is widened and deepened, some research[23] about fractional magnification has been done and it's working very well. We believe that methods based on deep learning will be more and more applicable to our real tasks. And it should be a reliable method can be used in a variety of tumors' digital slides, and will be available for a large scale in clinical pathology as an innovative technique.

Abbreviations

WSI: Whole Slide Image; CNN: Convolutional neural networks; DP : digital pathology ; AI: artificial intelligence; AGCT : adult granulosa cell tumor ; SR: super-resolution; GAN: generative adversarial network; CNNs: convolutional neural networks; SISR: Single Image Super-Resolution; PSNR: peak signal-to-noise ratio; SSIM: structural similarity; EDSR: Enhanced Deep Super-Resolution network; LR: low-resolution; HR: high-resolution; SRCNN: Super-Resolution Convolutional Neural Network.

Declarations

Acknowledgments

We thank all the pathologists and software engineers for participating in this study.

Author contributions

Ji Bao, Hong Bu designed the study.

Yang Deng, Min Feng collected and analyzed all the data.

Fei Xiang, Yizhe Wang provided the structure of super-resolution AI models.

Yang Deng, Yizhe Wang trained the super-resolution AI models.

Min Feng and Yong Jiang tested the model and gave there diagnosis from a doctor's point of view.

Yang Deng and Hangyu Qing analyzed the results and optimized the super-resolution AI models accordingly.

Yang Deng and Min Feng wrote the manuscript.

Funding

This work was supported by the National Key Research and Development Program (2017YFC0113908), the Technological Innovation Project of Chengdu New Industrial Technology Research Institute (2017-CY02-00026-GX), the 135 project for disciplines of excellence, West China Hospital (ZYGD18012) and Sichuan International Science and Technology Cooperation and Exchange Research and Development Project (2017HH0070 and 2018HH0037).

Availability of data and materials

The datasets used during the current study are available from the corresponding author on reasonable request.

Ethics approval and consent to participate

Data used in this study was collected as part of medical records. Institutional and/or national research ethic committee has approved the data collection and management process.

Competing interests

The authors declare no competing financial interests.

References

1. May M. A better lens on disease: Computerized pathology slides may help doctors make faster and more accurate diagnoses. Sci Am. 2010; 302: 74-77.
2. Irshad H, Veillard A, Roux L, et al. Methods for Nuclei Detection, Segmentation, and Classification in Digital Histopathology: A Review—Current Status and Future Potential. IEEE Rev Biomed Eng. 2014;7: 97-114.
3. Liang L, Ding YQ, Bian XW, et al., Development of telepathology in China, JSP-CSP Exchange Program Japan China: Joint Workshop at 2019 Annual Spring: Conference of JSP, Fukuoka, April 16-18, 2019[C] 2019.249
4. You CY, Li G, Zhang Y, et al. CT Super-resolution GAN Constrained by the Identical, Residual, and Cycle Learning Ensemble (GAN-CIRCLE). 2018. Available: https://arxiv.org/abs/1808.04256
5. Chaudhari A S, Fang Zhongnan, Kogan Feliks, et al., Super-resolution musculoskeletal MRI using deep learning. Magnetic resonance in medicine. 2018.
6. Chen YH, Shi F, Christodoulou AG, et al. Efficient and accurate mri super-resolution using a generative adversarial network and 3d multi-level densely connected network. In: International Conference on Medical Image Computing and Computer-Assisted Intervention. Springer 2018; pp: 91-99.
7. Chen YH, Xie YB, Zhou ZW, et al. Brain MRI super resolution using 3D deep densely connected neural networks. In: Biomedical Imaging (ISBI 2018), 2018 IEEE 15th International Symposium on, IEEE 2018; pp: 739-742
8. Chaudhari A S , Fang Z , Kogan F , et al. Super-resolution musculoskeletal MRI using deep learning[J]. Magnetic Resonance in Medicine, 2018.

9. Yinka F, Michael C, Olga W, et al. Adult Granulosa Cell Tumor With High-grade Transformation: Report of a Series With FOXL2 Mutation Analysis. Am J Surg Pathol. 2019 May 31. doi: 10.1097/PAS.0000000000001296.
10. Mills AM, Chinn Z, Rauh LA, et al. Emerging biomarkers in ovarian granulosa cell tumors. Int J Gynecol Cancer. 2019 Mar;29(3):560-565. doi: 10.1136/ijgc-2018-000065.
11. Bell SW, Kempson RL, Hendrickson MR. Problematic uterine smooth muscle neoplasms. A clinicopathologic study of 213 cases[J].Am J Surg Pathol. 1994, 18(6):535-558.
12. LeCun Y, Bengio Y, Hinton G. Deep learning. Nature 521, 436–444 (2015).
13. Esteva A, Kuprel B, Novoa RA, et al. Dermatologist-level classification of skin cancer with deep neural networks. Nature 542, 115–118 (2017).
14. Ryan P, Avinash VV, Katy B, et al. Prediction of cardiovascular risk factors from retinal fundus photographs via deep learning. Nat. Biomed. Eng. 2, 158–164 (2018).
15. Lim B, Son S, Kim H, et al. Enhanced deep residual networks for single image super-resolution. The IEEE conference on computer vision and pattern recognition (CVPR) workshops. Vol. 1. No. 2. 2017.
16. Chao D, Chen C L, Kaiming H, et al. Learning a deep convolutional network for image super-resolution. In: European Conference on Computer Vision. Springer. 2014, pp. 184–199.
17. Chao D, Chen C L, Tang XO. Accelerating the super-resolution convolutional neural network. In: European Conference on Computer Vision. Springer. 2016, pp. 391–407.
18. Shi WZ, Caballero J, Huszar F, et al. Real-time single image and video super-resolution using an efficient subpixel convolutional neural network. In: Proceedings of the IEEE Conference on Computer Vision and Pattern Recognition. 2016, pp. 1874–1883.
19. Timofte R, Agustsson E, Van Gool L, et al. Ntire 2017 challenge on single image super-resolution: Methods and results[C]//Proceedings of the IEEE Conference on Computer Vision and Pattern Recognition Workshops. 2017: 114-125.
20. https://cv.snu.ac.kr/research/EDSR/Presentation_v3(release).pptx.
21. Ledig C, Theis L, Huszar F, et al. Photo-Realistic Single Image Super-Resolution Using a Generative Adversarial Network. *CVPR*. Vol. 2. No. 3. 2017.
22. Mittal A, Moorthy A K, Bovik A C. No-reference image quality assessment in the spatial domain[J]. IEEE Transactions on Image Processing, 2012, 21(12): 4695-4708.
23. Hu X, Mu H, Zhang X, et al. Meta-SR: A Magnification-Arbitrary Network for Super-Resolution[J]. arXiv preprint arXiv:1903.00875, 2019.

Tables

Item	Detail
Input channels	3(RGB)
Input LR Patch size	256
Input HR Patch size	512
Mini-batch size	8
Learning rate	0.0001
Optimizer	ADAM(β1=0.9)
Loss	L1
# Residual blocks	16
# Filters	64
#Iteration epoch	300(2 days in single GTX 1080ti)
#Training images	8000
#Validating images	2000
Implementation	PyTorch

Table 1: Model specifications LR: low-resolution, HR: high-resolution, Adam: A Method for Stochastic Optimization

	sr_bilinear_as_lr_input	sr_self_as_lr_input
PSNR	43.92	42.03
SSIM	0.99	0.99

Table 2 Mean PSNR and SSIM values between the testing SR images and HR images

PSNR: peak signal-to-noise ratio, SSIM: structural similarity, sr_bilinear_as_lr_input: bilinear down-sampled images from 40× HR images, sr_self_as_lr_input: images directly from the 20× images in WSI

	GT_40×	SR_Bicubic_40×	SR_Ours_40×
BRISQUE	52.19	55.90	49.22

Table 3 Mean BRISQUE scores of HR images, SR images up-sampled by Bicubic and ours

BRISQUE : Blind/Referenceless Image Spatial QUality Evaluator, GT_40×: the HR images, SR_Bicubic_40×: super-resolution images related to Bicubic, SR_Ours_40×: super-resolution images related to ours

nuclear division dataset			nuclear groove dataset		
GT_40×	SR_Bicubic_40×	SR_Ours_40×	GT_40×	SR_Bicubic_40×	SR_Ours_40×
40.97	45.66	39.90	49.66	53.61	49.29

Table 4 Mean BRISQUE scores of HR images, SR images up-sampled by Bicubic and ours on nuclear division dataset and nuclear groove dataset

GT_40×: the HR images, SR_Bicubic_40×: super-resolution images related to Bicubic, SR_Ours_40×: super-resolution images related to ours

Opinion	Pathologist A		Pathologist B	
	uterine leiomyosarcoma	adult granulosa cell tumor	uterine leiomyosarcoma	adult granulosa cell tumor
There is no difference between HR and SR iamges	959	988	975	914
There is a marked difference between HR and SR iamges	41	12	25	86
Rate of SR images' authenticity	97.35%		94.45%	
Be confident to make a correct diagnosis based on SR images	951	988	977	925
Rate of diagnostic confidence	96.95%		95.1%	

Table 5 The subjective evaluations of the SR images from the pathologists

HR: high-resolution, SR: super-resolution

Results of test	Pathologist A		Pathologist B	
	uterine leiomyosarcoma	adult granulosa cell tumor	uterine leiomyosarcoma	adult granulosa cell tumor
HR image can be selected correctly	97	110	105	112
SR image was incorrectly selected	103	90	95	88
Accuracy	51.75%		54.25%	

Table 6 The objective test of the SR images from the pathologists

HR: high-resolution, SR: super-resolution

Figures

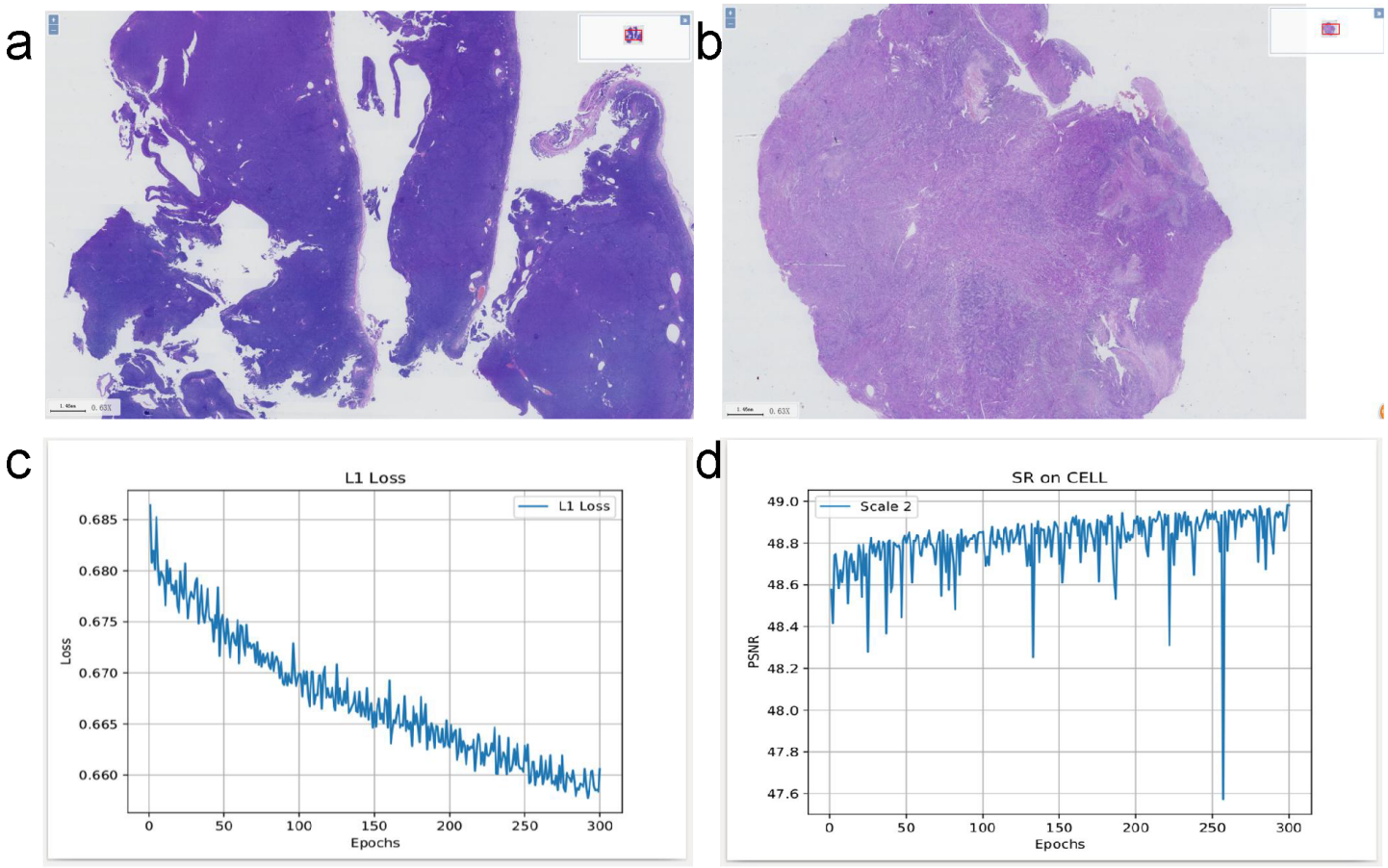

Figure 1

Examples of our datasets. a: Adult granulosa cell tumor, b: Leiomyosarcoma, c: Training loss curve, d: Curves of PSNR between the SR and HR images in validating dataset. PSNR: peak signal-to-noise ratio, SR: super-resolution, HR: high-resolution

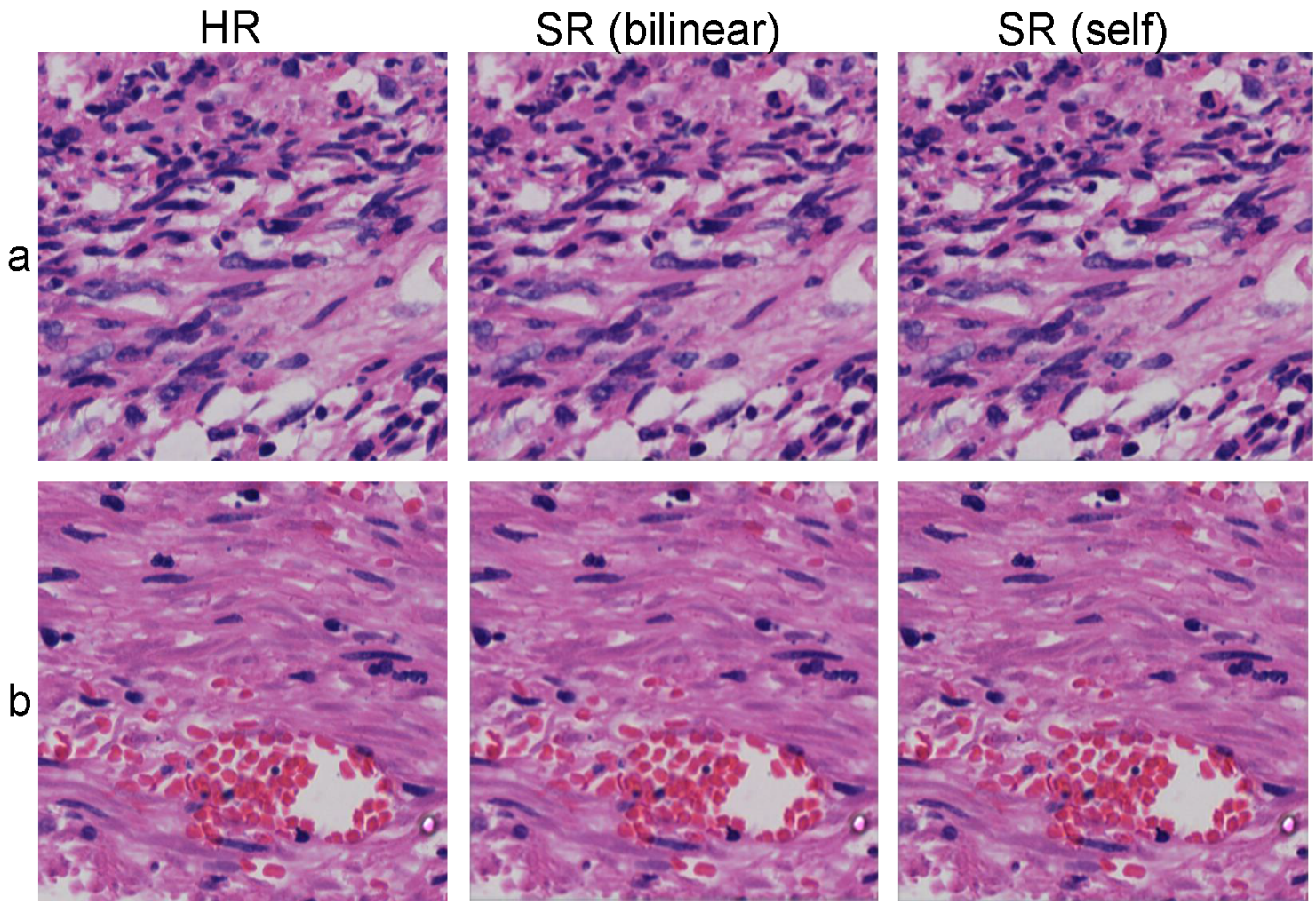

Figure 2

Result comparing between HR and SR images. Images from both a-b row are uterine leiomyosarcoma. The left column are HR images, the middle column are our SR images with sr_bilinear_as_lr_input, the right column are our SR images with sr_self_as_lr_input. SR: super-resolution, HR: high-resolution, sr_bilinear_as_lr_input: bilinear down-sampled images from 40× HR images, sr_self_as_lr_input: images directly from the 20× images in WSI

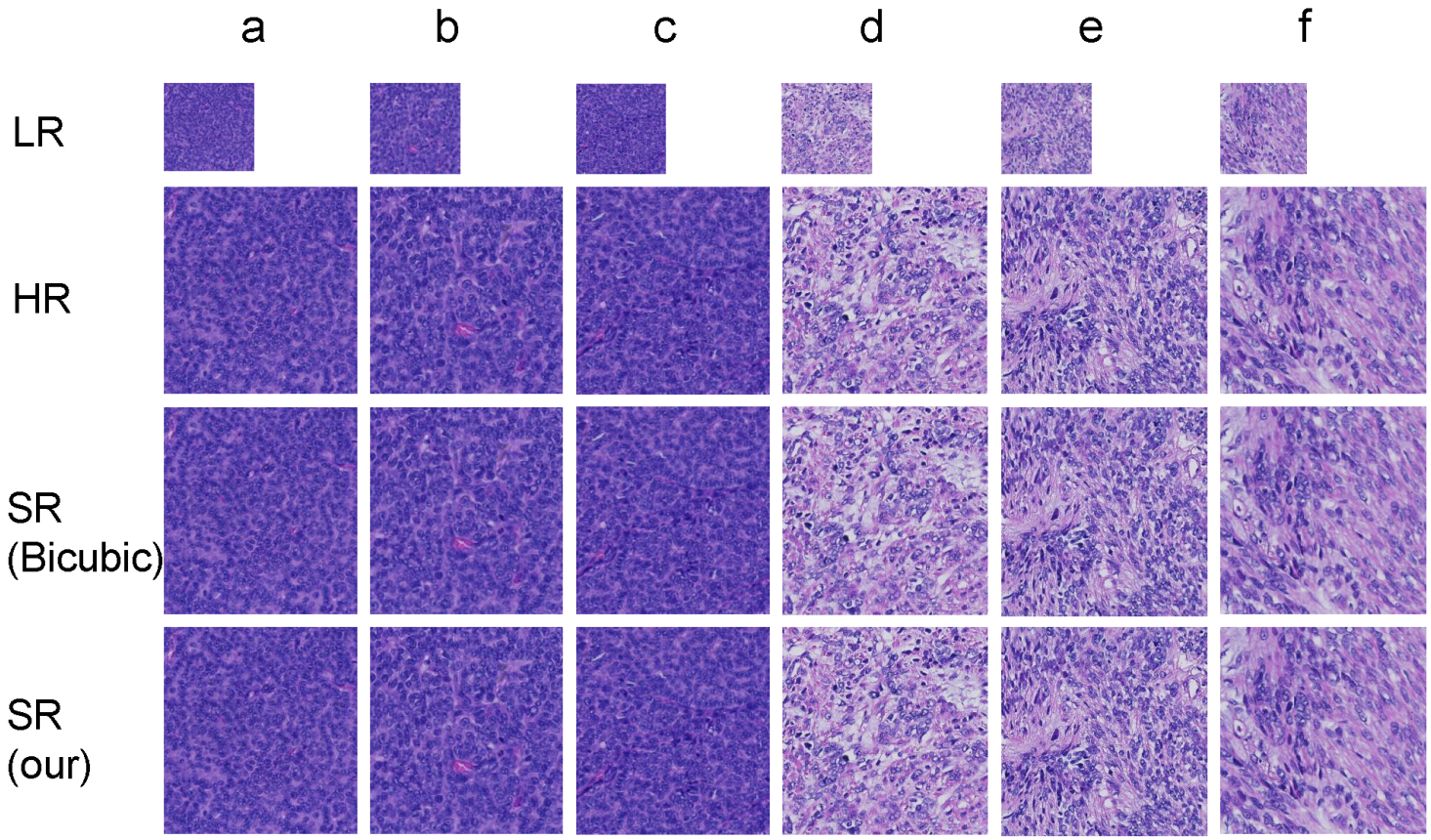

Figure 3

Result samples of AGCT and uterine leiomyosarcoma. The first row are LR images, the second row are HR images, the third row are the SR images up-sampled by Bicubic, the last row are our SR images. The a-c columns on the left are AGCT, and d-f columns on the right are uterine leiomyosarcoma. AGCT: adult granulosa cell tumor, LR: low-resolution, SR: super-resolution, HR: high-resolution

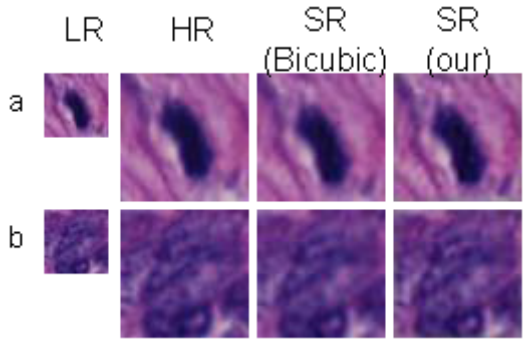

Figure 4

Result samples of nuclear division and nuclear groove. The a row are nuclear division images, the b row are nuclear groove images, the first column are LR images, the second column are HR images, the third column are the SR images up-sampled by Bicubic, the last column are our SR images. LR: low-resolution, SR: super-resolution, HR: high-resolution